HOSTED BY

ELSEVIER

Available online at www.sciencedirect.com

ScienceDirect

journal homepage: http://ees.elsevier.com/ejbas/default.asp

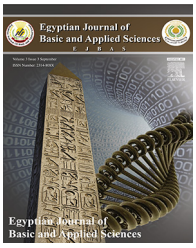

Full Length Article

Simulations of an all-optical flip-flop with a reset pulse frequency exceeding operating frequency

Hossam Zoweil *

Advanced Technology and New Materials Research Institute, City of Scientific Research and Technology Applications, New Borg EL-Arab City, P.O. Box 21934, Alexandria, Egypt

ARTICLE INFO

Article history:
Received 17 March 2016
Received in revised form 24 April 2016
Accepted 24 April 2016
Available online 10 May 2016

Keywords:
All-optical flip-flop
DFB laser
Optical nonlinearity
Urbach tail

ABSTRACT

An all-optical flip-flop based on a nonlinear multi-section DFB semiconductor laser structure is proposed. Holding beam is not required for device's operation. A section of the DFB structure is detuned to prevent lasing in the "OFF" state, and it is accompanied with a negative nonlinear coefficient that is due to partial absorption of photons at Urbach tail. At a high light intensity in the structure the nonlinear coefficient reduces the detuning, and the device is in lasing state; "ON" state. The device is reset by an optical pulse at a shorter wavelength through cross gain modulation. The reset pulse is absorbed in a middle section in the device before reaching the detuned nonlinear section. The switching times between the states are in nanoseconds time scale.

1. Introduction

All optical Internet requires all optical devices to process optical data directly (without conversion to electrical signal) in the optical domain. Particularly, all-optical flip-flops have roles as all optical memory elements, and these memory elements could be used in all optical data routing [1]. The all-optical flip-flop could be used for other applications such as optical shift register, optical random access memory and other applications [2]. Several schemes/devices are suggested for all-optical flip-flop devices. In [3], a device that is based on two coupled laser diode is presented. A device that is constructed from ring laser is presented in [4]. A device with two states of a clockwise and an anti-clockwise laser mode is introduced in [5]. Devices that are based on a semiconductor distributed feedback (DFB) laser, and on vertical cavity semiconductor optical amplifier (VCSOA) are shown in [6] and [7] respectively. All these devices require a holding beam or show output power in both states of the flip flop. Devices that have bistable optical output and do not require a holding beam are discussed in [8,9]. These devices have a saturable absorber in the laser cavity which has large optical loss at low light intensity in the laser cavity, and optical loss is reduced at high optical power intensity in the cavity.

In [10], a chirped DFB laser structure that behaves as an all-optical flip-flop is simulated. The flip-flop has a bi-stable output optical power behavior. The operation of the device does not require a holding beam. The chirped grating is accompanied by a linearly increasing negative nonlinear coefficient that is due to partial absorption of photons at the Urbach tail (The absorbed photons produce electron-hole pairs density that reduce the refractive index close to the band-gap energy). In the "OFF" state the chirp prevents constructive feedback from the grating and lasing does not occur. At high light intensity,

* Tel.: (002) 01223631091.
E-mail address: zoweil@gmail.com
http://dx.doi.org/10.1016/j.ejbas.2016.04.001

the chirp is reduced due to negative nonlinearity, and the laser mode builds up. The device is switched "OFF" by cross gain modulation. An optical pulse of a wavelength longer than the operating wavelength reduces the gain of the active layer, and in the same time does not produce much change in the refractive index (lower absorption coefficient at a longer wavelength).

In this work, a new design for an all-optical flip-flop is simulated. Instead of the chirped grating accompanied with a linear increasing negative nonlinear coefficient, a part of the wave-guiding grating of the suggested device is detuned from the rest of the grating. The detuned part has a slightly higher refractive index than the rest of the grating and has a negative nonlinear coefficient. The negative nonlinear coefficient is due to partial absorption of photons at the Urbach tail. The structure investigated in this work is easier to fabricate than the structure mentioned in [10] because only one nonlinear section is needed to achieve optical bistability in the laser device. The switch OFF ("Reset") mechanism is done by cross gain modulation (XGM), and a "Reset" pulse at a wavelength shorter than the wavelength of the "Set" pulse is used. The "Reset" pulse has a higher frequency (shorter wavelength) than the "Set" pulse and the operating frequency, which produces more design flexibility. This is in contrast to the device in [10], where the the "Reset" pulse has to be at a lower frequency than the operating frequency. In the next section the device schematic is presented and the flip-flop design is discussed.

2. Device schematic and description

The suggested device consists of a nonlinear DFB laser structure. The refractive index distribution along the wave-guiding layer of the device is shown in Fig. 1. The grating period is adjusted as $2\bar{n}d = \lambda_G$, where $\bar{n}$ is the average refractive index along the grating, d is the grating period, λ_G is the wavelength at the center of the reflection band of the grating. The device has a phase shift section in the middle of the grating. The optical gain is provided by electrical current injected into the active layer along the wave-guiding layer. The negative nonlinear coefficient is due to direct absorption of photons at the Urbach tail at a photon energy slightly less than the semiconductor band-gap energy in the nonlinear section. The loss coefficient at the Urbach tail is expressed as: $\alpha(\omega) = \alpha_0 \times exp((\hbar\omega - \hbar\omega_g)/E_0)$ [11,12], $\hbar\omega_g = E_g$ is the band gap energy, $\hbar$ is the Plank's constant (The energies are expressed in electron volt). The absorbed photons produce electron-hole pairs that reduce the refractive index at a photon energy slightly less than the semiconductor band-gap. At low optical power intensity in the structure, the detuned part of the wave-guiding layer reduces the available optical feedback to the laser mode, and the laser mode does not build up. To set the flip-flop "ON", an optical pulse of wavelength $\lambda = \lambda_1$ is injected, at $z = 0$, where $\lambda_1 = \lambda_G$. The semiconductor band gap energy E_g in the nonlinear section is adjusted such that the photons energies at $\lambda = \lambda_1$ is slightly less than E_g. Fig. 2 shows the gain spectrum of the device [13], the "Set" and "Reset" pulses frequencies (wavelengths), and the optical loss at Urbach tail. The injected "Set" pulse induces electron-hole pair densities in the nonlinear section and reduces its refractive index and its detuning; hence it provides extra optical feedback to photons of wavelength around $\lambda = \lambda_1$, the optical mode builds up and provides optical power (photons) that produce electron-hole pairs in the nonlinear section and maintain the reduction in the detuning in that section.

To reset the flip-flop, an optical pulse at $\lambda = \lambda_2$ is injected at $z = 0$. In this work we choose $\lambda_2 < \lambda_1$, which means that the reset pulse will be absorbed in the nonlinear section and may prevent the flip-flop from switching "OFF" properly. At $L/2 < z < 3L/4$ along the wave-guiding layer, the band-gap of the wave-guiding layer is altered to provide large absorption to photons of wavelength $\lambda = \lambda_2$ (Fig. 3). In Section "1", the band gap energy is higher than "Set/Reset" pulse photons energies. In section "2", the "Reset" pulse will be absorbed because the band gap energy is lower than the "Reset" pulse photon energy. The "Reset" pulse energy is totally absorbed in section "2" before it reaches section "3". Section "3" is the detuned

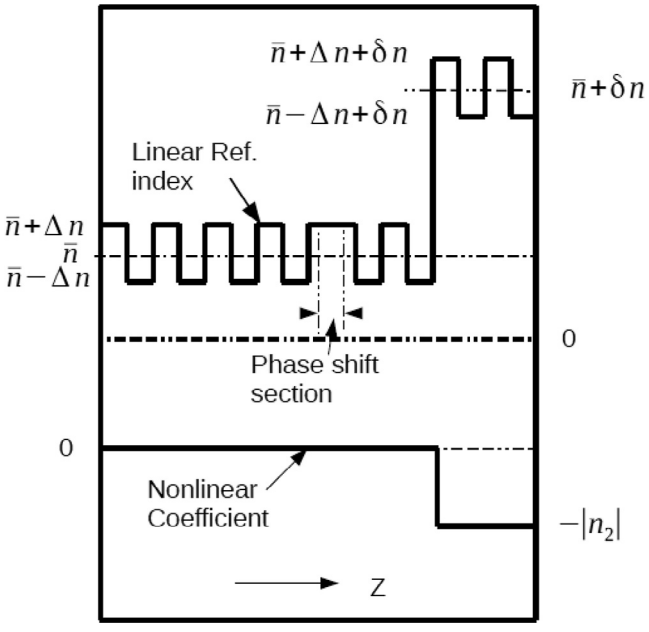

Fig. 1 – Linear refractive index and nonlinear coefficient distribution.

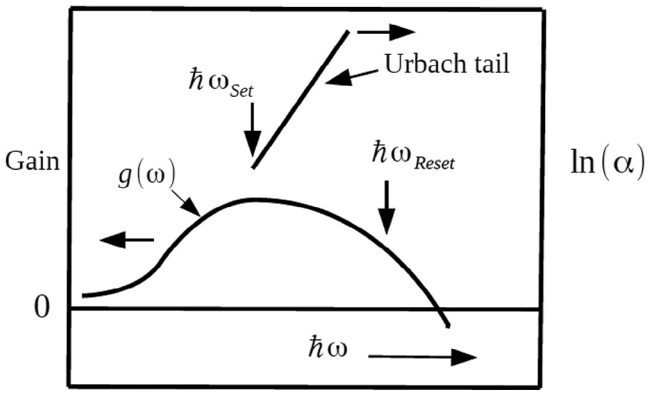

Fig. 2 – Gain spectrum, Urbach tail loss and "Set/Reset" pulses frequencies (wavelengths).

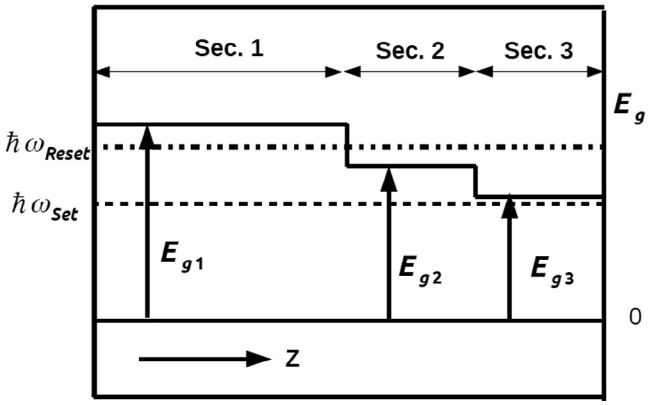

Fig. 3 – Energy gap of the semiconductor wave-guiding layer along the device; section "3" is the nonlinear wave-guiding section.

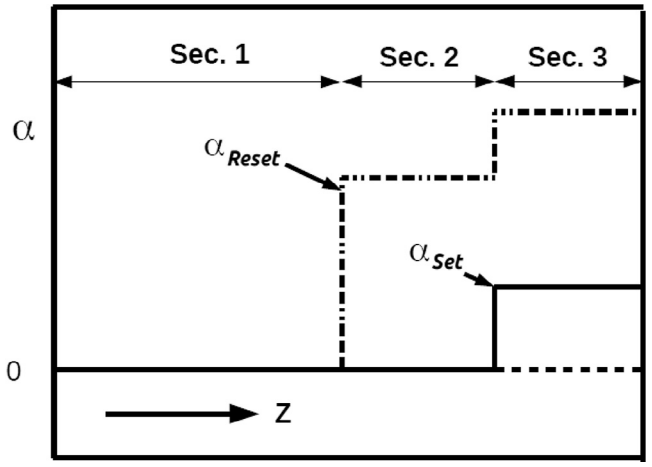

Fig. 4 – Energy gap of the semiconductor wave-guiding layer along the device.

grating section, its band gap energy is slightly higher than the "Set" pulse photon energy and the output laser mode photon energy. The absorption loss α_{Set} at the "Set" pulse frequency ($\omega = \omega_1$ or $\lambda = \lambda 1$), and the absorption loss α_{Reset} at the "Reset" pulse frequency ($\omega = \omega_2$ or $\lambda = \lambda 2$) are plotted in Fig. 4.

In this work it was assumed $\lambda_1 = 1500$ nm and $\lambda_2 = 1450$ nm (Window of low absorption loss in optical fiber). The reset pulse reduces the optical gain of the laser mode by XGM, and it is absorbed in section "2". Whence the optical laser mode gain is reduced the light intensity at $\lambda = \lambda_1$ is reduced and electron-hole density in section "3" decays toward zero, the optical feedback in the cavity is reduced and the device is switched OFF. In the next sections, a mathematical model of the device is presented an solved numerically. "Set/Reset" dynamics are simulated in time domain and results are discussed.

3. Mathematical model and simulations parameters

To simulate the switching dynamics in the structure coupled mode equations are used to model optical fields inside the structure [14]. The optical modes are coupled with rate equations. The total optical field is expressed as: $E(z,t) = E_+(z,t)\exp[i\beta z - i\omega t] + E_-(z,t)\exp[-i\beta z - i\omega t] + \text{c.c.}$. The optical laser mode is modeled at $\omega = \omega_1$. $\beta = 2\pi\bar{n}/\lambda_G$.

The "Reset" pulse angular frequency ω_2 is far detuned from reflection band of the grating. The "Reset" pulse optical field in the structure has only a propagating component in the $+ve$ z direction and is expressed as $E_{Reset} = E(z,t)_R \times \exp[i\beta z - i\omega t] + \text{c.c.}$, and $\omega = \omega_2$. It is assumed that the reset pulse is amplified in the first section ($0 < z < L/2$), and it is attenuated in the second section ($L/2 < z < 3L/4$). Due to large attenuation constant in the second section (compared to optical gain provided by the active layer), only loss coefficient is applied to the "Reset" pulse in the second section. In section "2", it is assumed the propagating reset pulse optical power is multiplied by $\exp\left[-\int_{L/2}^{z}\alpha(\omega_2)dz\right]$. It is assumed that the "Reset" pulse is completely consumed in the second section, and no "Reset" signal propagates in the third section. The equations that model the all-optical flip-flop are as follows:

$$\frac{\partial E_+}{\partial z} + \frac{\bar{n}}{c}\frac{\partial E_+}{\partial t} = \left(i\Gamma_1 + \frac{g}{2}(1+i\gamma) - \frac{\alpha_{cav}}{2}\right)E_+ + (i\Gamma_2\exp[i\phi(z) + i2\delta\beta z])E_- \quad (1)$$

$$\frac{\partial E_-}{\partial z} - \frac{\bar{n}}{c}\frac{\partial E_-}{\partial t} = -\left(i\Gamma_1 + \frac{g}{2}(1+i\gamma) - \frac{\alpha_{cav}}{2}\right)E_- - (i\Gamma_2\exp[-i\phi(z) - i2\delta\beta z])E_+ \quad (2)$$

$$\frac{\partial E_R}{\partial z} + \frac{\bar{n}}{c}\frac{\partial E_R}{\partial t} = \left(i\Gamma_1 + \frac{g}{2}(1+i\gamma) - \frac{\alpha_{cav}}{2}\right)E_R \quad (3)$$

$$\Gamma_1 = \frac{2\pi}{\lambda_G}\left(\delta n(z) - \left|\frac{dn}{dN}\right|N_c(1-i\xi)\right) + i\frac{\alpha(z,\omega_{1,2})}{2} \quad (4)$$

$$\Gamma_2 = \frac{4}{\lambda_G}\Delta n \quad (5)$$

$$\frac{\partial N_c(z,t)}{\partial t} = -\frac{N_c}{\tau_c} - BN_c^2 - CN_c^3 + \frac{\alpha(z,\omega_1)I_1}{\hbar\omega_1} + \frac{\alpha(z,\omega_2)I_2}{\hbar\omega_2} \quad (6)$$

$$\frac{\partial N_g(z,t)}{\partial t} = \frac{I_{current}}{qV} - \frac{N_g}{\tau_g} - BN_g^2 - CN_g^3 - v_g\Theta(g(\omega_1)S_1 + g(\omega_2)S_2) \quad (7)$$

$$g(\omega_{1,2}) = \frac{g(\tilde{\omega}_{1,2})(N_g - N_{tr})}{1 + \epsilon(S_1 + S_2)} \quad (8)$$

Equations 1 and 2 present the two counter propagating modes in the device. Equation 3 describes the "Reset" pulse propagation in the structure. Γ_1 presents the detuning along the structure due to optical gain change and refractive index change, and it presents the optical loss in the cavity. Γ_2 is the coupling between forward mode and backward mode. In the simulations $c = 3\times10^8$ m/s. $\bar{n} = 3$ is the average refractive index along the structure. $\Delta n = 0.001$, and $\delta n = 0.006$, for $3L/4 < z < L$ and 0 otherwise. The optical nonlinearity in the nonlinear section (Section "3") is due to direct absorption of photons at $\omega = \omega_1$. A part of photons is absorbed and electron-hole pairs are generated. The electron-hole pairs generated reduce

Table 1 – Simulation parameters.

Symbols	Description	Value
L	Length	187.5 μm
$I_{current}$	Current injected in the active layer	0.095523 Ampere
$\bar{n}$	Average ref. index	3
v_g	Group velocity	10^8 m/s
α_{cav}	Intrinsic cavity loss	25 cm_{-1}
γ	Line-width enhancement	–0.5
ε	Gain saturation	1.5×10^{-23} m^3
Θ	Overlap factor	0.35
V	Cavity volume	0.36×10^{-16} m^3
τ_{car}	Non-radiative recombination in nonlinear sections	1 ns
τ_g	Non-radiative recombination in the active layer	3 ns
B	Radiative recombination	10^{-23} m^3/s
C	Auger recombination	3×10^{-40} m^6/s
$g(\tilde{\omega}_1)$	Differential gain at ω_1	4×10^{-20} m^2
N_{tr}	Transparency carrier density	10^{23} m^{-3}

the refractive index at photon energies just below the energy gap of the semiconductor. At photon energy below the band gap energy the loss follows Urbach tail expression [12], $\alpha(\omega)=\alpha_0\times exp((\hbar\omega-\hbar\omega_g)/E_0)$, $\hbar\omega_g=E_g$, E_0 is around 0.01 eV. In this simulation $\alpha(\omega_1)=480\ cm^{-1}$ for $3L/4<z<L$ and 0 otherwise. $\alpha(\omega_2)=9600\ \mathrm{cm}^{-1}$, for $L/2<z<3L/4$ and 0 otherwise. The change in the refractive index due to the change in the electron-hole density is $-|dn/dN|\times N_c$, and $-|dn/dN|=-10^{-26}\ \mathrm{m}^3$ [15,16]. $\xi=0.03$ is the ratio between the change in the refractive index to the change in the optical loss due to the generated electron hole density [16]. I_1 and I_2 are the optical power density on the "Set" pulse (optical laser mode at ω_1) and the "Reset" pulse (at ω_2) respectively. S_1 and S_2 are the photons densities in the laser cavity at ω_1 and ω_2 respectively. $\phi=0$ for $0<z<$ / $L/2$, and $\phi=\pi$ otherwise. It was assumed $g(\tilde{\omega}_2)=0.5\times g(\tilde{\omega}_1)$. Other simulation parameters are shown in Table 1.

The structure is divided into 80 sections. In each section, the forward and backward fields are calculated using Rung-Kutta methods. The electron hole densities in the waveguiding layer and the active layer are calculated with the same methods. In each step, random fields are added to the backward and forward mode to model the spontaneous emissions. To reduce the simulation time, the simulations are performed on a general purpose graphics processing unit (GPGPU). In each time step, the calculation load is distributed among 80 parallel threads; a thread per each section along the length of the structure (one can assign more threads per section). The integration step along the z axis is $L/80$, and the time step is $\bar{n}L/c80$. The work is performed on a PC machine 32 GB, processor: Intel Core i3-4130 CPU @ 3.40 GHz × 4, GPGPU: Geforce GTX 670. The simulation code is written using CUDA C [17]. The simulation's time on PC is reduced 20 times by using GPGPU computing. In the following sections results and numerical simulations of the device are shown.

4. Numerical simulations and results

In the following simulation the output optical field is normalized to $P_0=0.05\times10^{-3}$ watt. N_g is normalized to N_{th}. N_c is normalized to $N_0=10^{23}\ m^{-3}$.

4.1. *Optical bi-stability loop*

To determine the required injected current to obtain two stable optical level output (at the same injected current) a numerical experiment is performed. The injected current is increased linearly from zero to 0.122 Ampere in 75 ns, then the injected current is reduced again to 0 linearly in 75 ns. At part of the current versus optical output relation is plotted in Fig. 5. In the following simulations, the injected current $I=95.523$ mA is assumed. It insures bistable operation of the device.

4.2. *"OFF" state and "ON" state*

The output optical power in the "OFF" state at $z=L$ is simulated in time domain for 75 ns, Fig. 6(a). The "ON" state is triggered by an input pulse injected at $z=0$, of power $P=P_0$ and time width $t=187.5$ picosecond (9.375×10^{-3} picojule). The device is triggered at $t=7.5$ ns from the start of the simulation time, the output optical power at $z=L$ is shown in Fig. 6(b). The injected pulse at $\omega=\omega_1$ is amplified along the structure

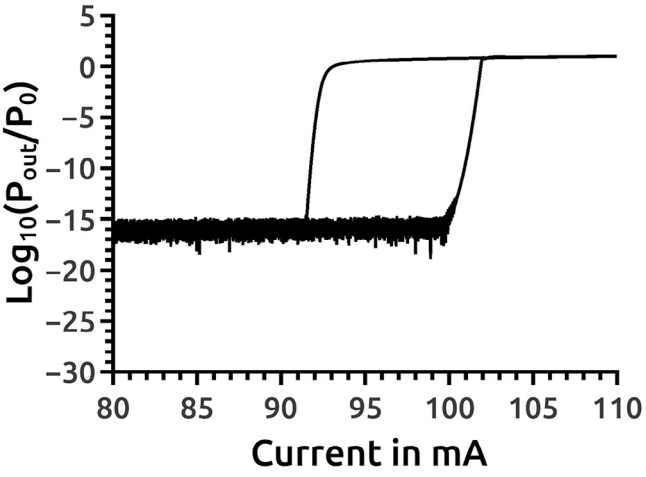

Fig. 5 – Optical bi-stability loop, injected current versus $Log_{10}(P_{out}/P_0)$.

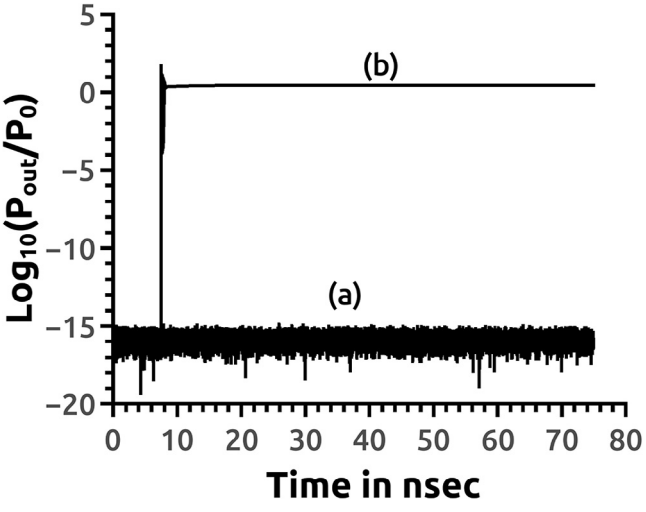

Fig. 6 – Output optical power in; (a) "OFF" and (b) "ON" states simulations in time domain.

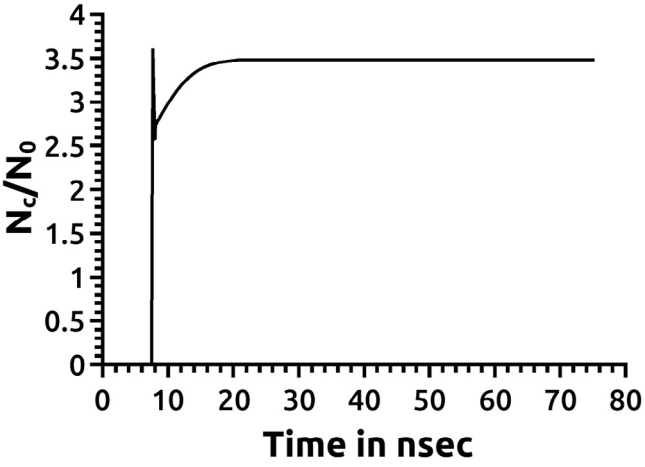

Fig. 7 – N_c/N_0 evolution at z = 7L/8.

and a part of photons is absorbed at the Urbach tail in the third section (the nonlinear section). The absorbed photons generate electron-hole pairs that reduce the refractive index of that section. As the detuning of this section decreases, the grating in this section starts to reflect back more photons back to the device and decreases the number of photons leaving the device at $\omega = \omega_1$. The optical feedback along the structure increases and the laser mode at $\omega = \omega_1$ builds up. As the optical power of the laser mode builds up, it maintains the number of photons in section 3 that are required to generate the electron hole density needed to set the detuning of this section to a low value.

The electron hole density N_c normalized to N_0 in the nonlinear section (Section 3) at ($z = 7L/8$), is shown in Fig. 7. The electron hole density in the active layer N_g normalized to N_{th} is plotted in Fig. 8 at $z = 7L/8$.

$(\delta n - |dn/dN| \times N_c)/\Delta n$ is plotted in Fig. 9. It shows the relative changes in the refractive index in the nonlinear section after 75 ns in the "OFF" and in the "ON" states at $z = 7L/8$.

4.3. *"ON/OFF" transitions dynamics*

"ON/OFF" transitions are simulated in time domain. A "Set" pulse followed by a "Reset" pulse are injected to the structure

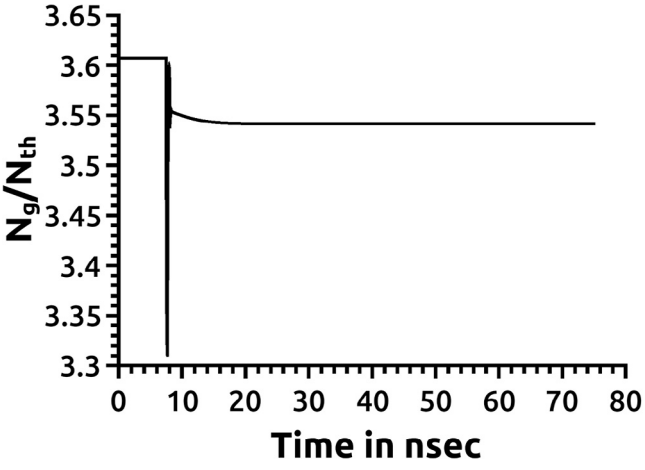

Fig. 8 – N_g/N_{th} evolution at z = 7L/8.

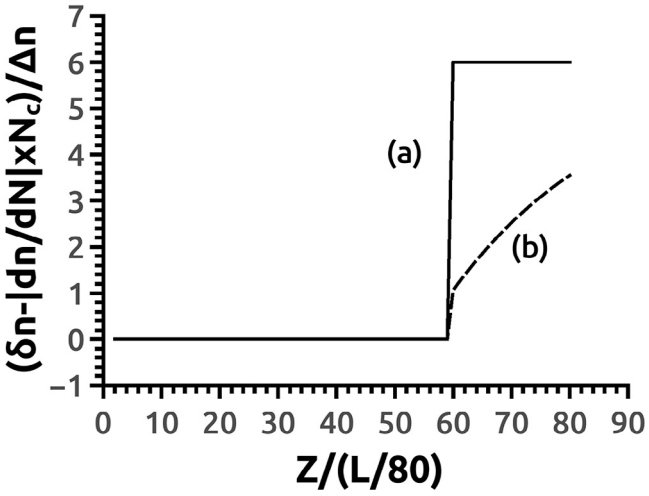

Fig. 9 – Relative change in the refractive index in (a) "OFF" and (b) "ON" states after 75 ns.

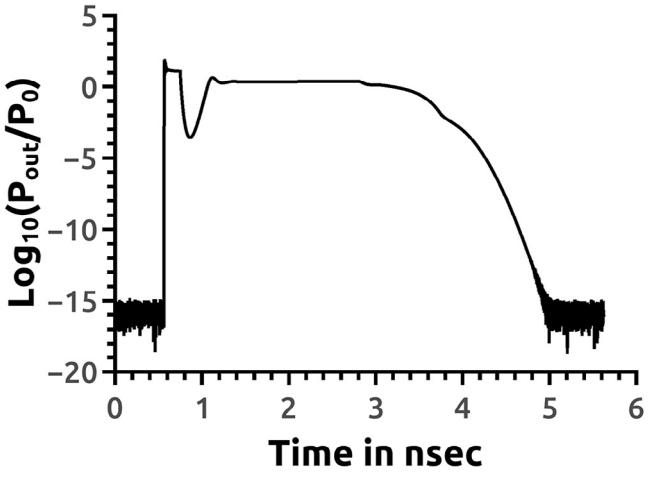

Fig. 10 – Output optical power during "ON/OFF" ("Set/Reset") operations.

at $z = 0$, and the optical fields are simulated for 5.625 ns. A "Set" pulse of power $P = P_0$ and width 0.1875 ns (9.375×10^{-3} picojule), at $\omega = \omega_1$ and t = 0.5625 ns switches the flip-flop "ON". Another pulse at t = 2.8125 ns, of power $P = P_0$, pulse width 0.9375 ns ($\omega = \omega_2$, 46.875×10^{-3} picojule) switches the Flip-Flop "OFF". The output field at $z = L$ is shown in Fig. 10. The evolution of N_c/N_0, and N_g/N_{tr} with time at $z = 7L/8$ are shown in Figs. 11 and 12 respectively.

The "Reset" pulse at $\omega = \omega_2$ is amplified in the first half of the device. In section "2", the pulse is absorbed almost completely due to large attenuation coefficient. The amplification of pulse in that section is neglected compared to the large attenuation by the semiconductor of band gap $E_g < \hbar\omega_2$. The "Reset" pulse reduces the gain of the optical laser mode at $\omega = \omega_1$ by XGM. When the optical gain of the laser mode is reduced, the photons absorbed in section "3" are reduced, and also the electron hole pairs generated in the wave-guiding layer in that section are reduced, the refractive index increases and the detuning is restored to its value in the "OFF" state. The

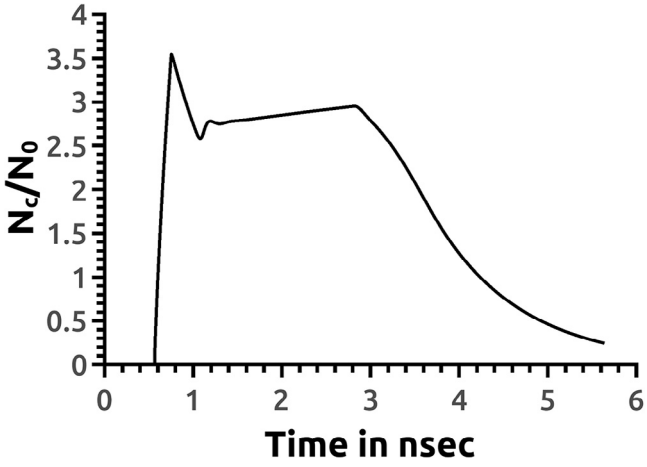

Fig. 11 – N_c/N_0 evolution during "Set/Reset" operation at $z = 7L/8$.

"Reset" pulse at $\omega = \omega_2$ is totally absorbed in section "2", it does not reach section "3", and does not affect the electron hole densities in section "3". As the "Reset" pulse is absorbed in section "2", it generates electron hole pairs that changed the detuning for the laser mode along that section. The refractive index distributions during "Set/Reset" operation in both sections "2" and "3" at successive time frames are shown in Fig. 13.

4.4. *Multiple "Set/Reset" operations*

Multiple "Set/Reset" operations are simulated in the time domain for 45 ns. The input pulses at $z = 0$ are shown in Fig. 14. Each "Set" pulses is followed by a "Reset" pulse after 9 ns. "Reset" pulse is followed by a "Set" pulse after 6 ns. The input "Set" pulse of $P = P_0$ has pulse width 0.1875 ns (9.375×10^{-3} picojoule at $\omega = \omega_1$). The "Reset" pulse of $P = P_0$ has pulse width 0.9375 ns (46.875×10^{-3} picojoule at $\omega = \omega_2$) switches the Flip-Flop "OFF". The output optical power at $z = L$ is shown in Fig. 15. The time evolution of N_c/N_0 $z = 7L/8$ during multiple "Set/Reset" operations is shown in Fig. 16. N_g/N_{tr} time evolution is plotted in Fig. 17.

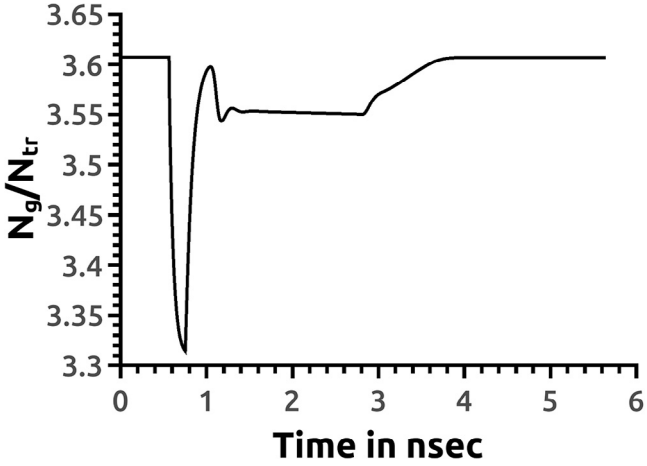

Fig. 12 – N_g/N_{tr} evolution during "Set/Reset" operation at $z = 7L/8$.

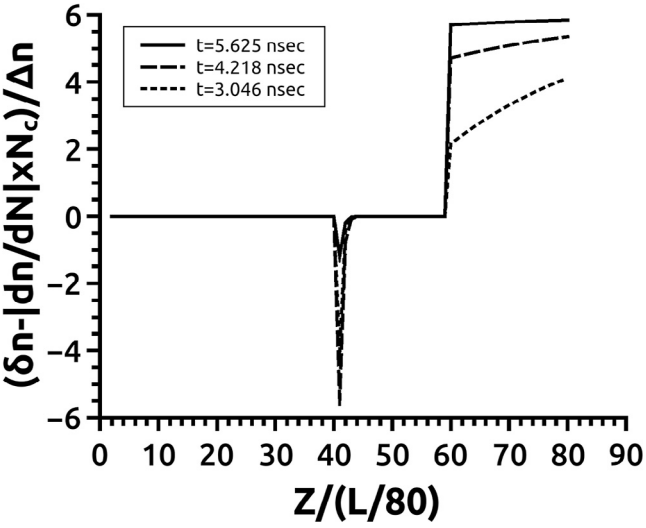

Fig. 13 – Refractive index distributions during "Set/Reset" operations at different time frames.

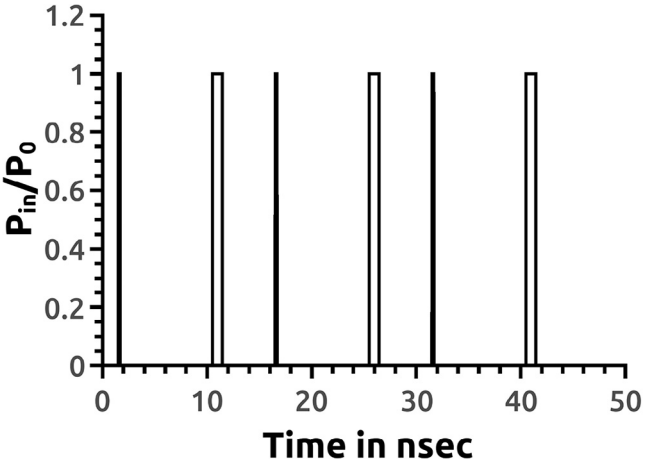

Fig. 14 – Input signal.

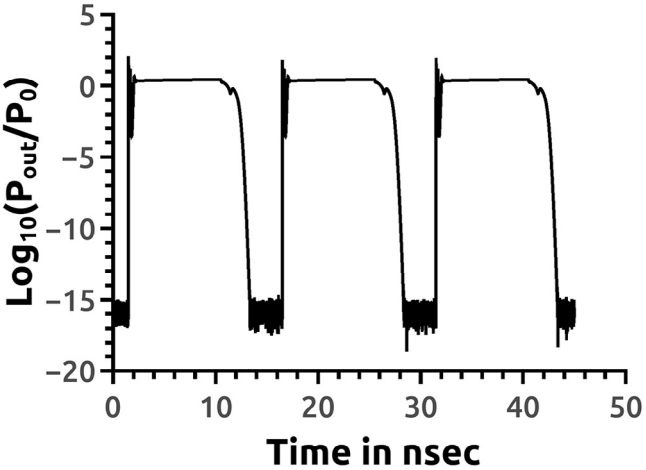

Fig. 15 – Output optical field at $z = L$.

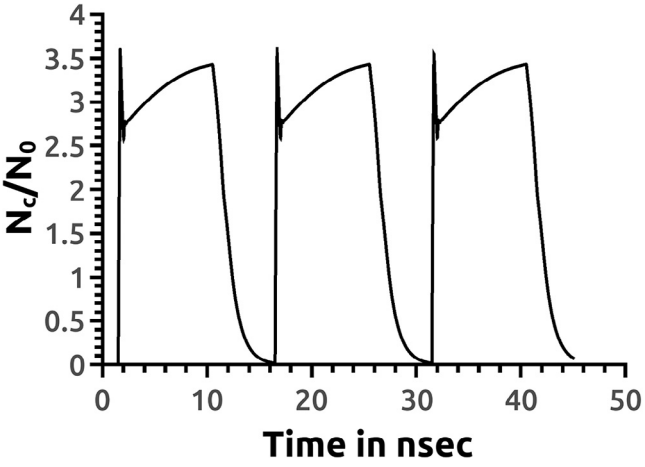

Fig. 16 – N_c/N_0 evolution with time at $z = 7L/8$.

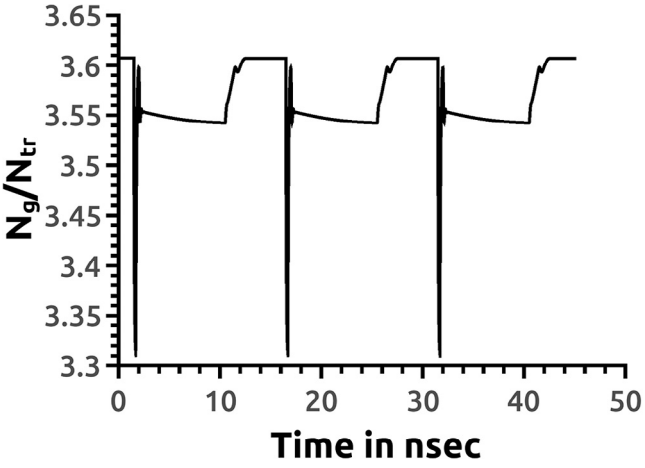

Fig. 17 – N_g/N_{th} evolution with time at $z = 7L/8$.

5. Discussion

The device operation requires altering the band gap of the semiconductor material in the wave-guiding layer. This could be done as the device is fabricated from *InGaAsP* alloy on *InP* substrate. By changing the percentage of the *InGaAsP* alloy ingredient, the band gap could be changed [18]. The extinction ratio is $Log_{10}(P_{ON}/P_{OFF}) \simeq -15$, and no holding beam is required for bi-stable operation. During "Set" operation the output optical field takes 0.5 ns to stabilize; however N_c takes about 10 ns to reach its steady state value ($N_c/N_0 = 3.5$) (Fig. 7); however, an input pulse with higher energy can lead N_c to reach steady state in a shorter time. During "Set/Reset" operation (Fig. 10), a "Reset" pulse of width 0.9375 ns is injected to the device; however, the output optical output power takes about 2 ns to reach the optical level of the "OFF" state. The "Reset" dynamics in time domain are shown during N_c transition state (before N_c reaches transition state) in case of single "ON/OFF" (or "Set/Reset") operation (Figs. 10–12) and at the end of N_c transition state (9 ns after "Set" pulse) during multiple "Set/Reset" operation (Figs. 15–17).

6. Conclusion

In this work, an all-optical flip-flop based on a non-linear semiconductor DFB laser structure is introduced. The "Reset" mechanism uses an optical pulse of a shorter wavelength than the "Set" pulse wavelength. The device could be built using *InGaAsP* alloy. Simulations show that a "Set" pulse of 0.1875 ns pulse width switched the device "ON" and optical mode stabilizes in 0.5 ns. A "Reset" pulse of 0.9375 ns pulse width switches the device "OFF" in 2 ns. The switching dynamics are in nanoseconds time scale and it is suitable for all optical data packets routing.

REFERENCES

[1] Dorren HJS, Hill MT Liu, Y, Calabretta N, Srivatsa A, Huijskens FM, et al. Optical packet switching and buffering by using all-optical signal processing methods. J Lightwave Technol 2003;21(1):2–12.
[2] Li P, Wang Y, Zhang J. All-optical fast random number generator. Opt Express 2010;18(18):20360–9.
[3] Martin T, de Waardt H, Khoe GD, Dorren HJS. All-optical flip-flop based on coupled laser diodes. IEEE J Quant Electron 2001;37(3):405–13.
[4] Hill MY, Dorren HJ, De Vries T, Leijtens XJ, Den Besten JH, Smalbrugge B, et al. A fast low-power optical memory based on coupled micro-ring lasers. Nature 2004;432:206–8.
[5] Liu L, Kumar R, Huybrechts K, Spuesens T, Roelkens G Geluk EJ, et al. An ultra-small, low-power, all-optical flip-flop memory on a silicon chip. Nature Photon 2010;4:182–7.
[6] Huybrechts K, Morthier G, Baet R. Fast all-optical flip-flop based on a single distributed feedback laser diode. Opt Express 2008;16:11405–10.
[7] Kaplan AM, Agrawal GP, Maywar DN. All-optical flip-flop operation of VCSOA. Electron Lett 2009;45(2):127–8.
[8] Kawaguchi H. Bistable laser diodes and their applications: state of the art. IEEE J Sel Top Quantum Electron 1997;3(5):1254–70.
[9] Odagawa T. Bistable semiconductor laser diode device, US Patent, 5007061, 9 April, 1991.
[10] Zoweil H. Numerical simulation of a novel all-optical flip-flop based on a chirped nonlinear distributed feedback semiconductor laser structure using GPGPU computing. J Mod Opt 2015;62(9):738–44.
[11] Pankove JI. Absorption edge of impure gallium arsenide. Phys Rev 1965;140(6A):A2059–65.
[12] Dow JD, Redfield D. Toward a unified theory of Urbach's rule and exponential absorption edges. Phys Rev B 1972;5:594–610.
[13] Agrawal GP, Dutta NK. Semiconductor lasers. New York: Kluwer Academic Publisher; 2003.
[14] Carrol J, Whiteaway J, Plumb D. Distributed feedback semiconductor laser. London: IEE; 1998.
[15] Bennett BR, Soref RA, Del Alamo JA. Carrier-induced change in refractive index of InP, GaAs, and InGaAsP. IEEE J Quant Electron 1990;26(1):113–22.
[16] Haug H editor. Optical nonlinearities and instabilities in semiconductors. New York: Academic Press; 1988.
[17] Programming Guide (PDF) – v7.5 – Last updated September 1, 2015. Copyright © 2007–2015 NVIDIA Corporation <https://docs.nvidia.com/cuda/pdf/CUDA_C_Programming_Guide.pdf>.
[18] Adachi S. Physical properties of III-V semiconductor compounds: InP, InAs, GaAs, GaP, InGaAs, and InGaAsP. New York: Wiley; 1992.